

ENSO-Driven Variability of Denitrification and Suboxia in the Eastern Tropical Pacific Ocean

Journal Article**Author(s):**

Yang, Simon; Gruber, Nicolas ; Long, Matthew C.; Vogt, Meike

Publication date:

2017-10

Permanent link:

<https://doi.org/https://doi.org/10.3929/ethz-c-000211898>

Rights / license:

[In Copyright - Non-Commercial Use Permitted](#)

Originally published in:

Global Biogeochemical Cycles 31(10), <https://doi.org/10.1002/2016GB005596>

RESEARCH ARTICLE

10.1002/2016GB005596

Key Points:

- ENSO alters water column denitrification in the Eastern Tropical Pacific by up to 70%
- These changes are driven by variations in oxidant demand and heaving of the oxic-suboxic boundary
- The changes in the suboxic zone are primarily caused by wind-driven variations in tropical circulation

Supporting Information:

- Figure S1
- Figure S2
- Figure S3
- Figure S4
- Figure S5
- Figure S6
- Figure S7
- Figure S8
- Supporting Information S1

Correspondence to:

S. Yang,
simon.yang@usys.ethz.ch

Citation:

Yang, S., Gruber, N., Long, M. C., & Vogt, M. (2017). ENSO driven variability of denitrification and suboxia in the Eastern Tropical Pacific Ocean. *Global Biogeochemical Cycles*, 31, 1470–1487. <https://doi.org/10.1002/2016GB005596>

Received 6 DEC 2016

Accepted 4 SEP 2017

Accepted article online 15 SEP 2017

Published online 18 OCT 2017

ENSO-Driven Variability of Denitrification and Suboxia in the Eastern Tropical Pacific Ocean

Simon Yang¹ , Nicolas Gruber¹ , Matthew C. Long² , and Meike Vogt¹ 

¹Environmental Physics, Institute of Biogeochemistry and Pollutant Dynamics, ETH Zürich, Zürich, Switzerland, ²National Center for Atmospheric Research, Boulder, CO, USA

Abstract The Eastern Tropical Pacific (ETP) hosts two of the world's three Oxygen Deficient Zones (ODZs), large bodies of suboxic water that are subject to high rates of water column denitrification (WCD). In the mean, these two ODZs are responsible for about 15 to 40% of all fixed N loss in the ocean, but little is known about how this loss varies in time. Here we use a hindcast simulation with the ocean component of the National Center for Atmospheric Research (NCAR) Community Earth System Model over the period 1948 to 2009 to show that the El Niño–Southern Oscillation (ENSO) drives large variations in the rates of WCD in this region. During mature La Niña (El Niño) conditions, peak denitrification rates are up to 70% higher (lower) than the mean rates. This large variability is the result of wind-driven changes in circulation and isopycnal structure concurrently modifying the thermocline distribution of O₂ and organic matter export in such a way that the response of WCD is strongly amplified. During average La Niña (El Niño) conditions, the overall changes in ODZ structure and primarily the shoaling (deepening) of the upper boundary of both ODZs by 40 to 100 m explains 50% of the changes in WCD in the North Pacific and 94% in the South Pacific. Such a large variability of WCD in the ETP has strong implications for the assessments of trends, the balance of the marine N cycle and the emission of the greenhouse gas N₂O.

1. Introduction

Anthropogenic climate change is projected to drive deoxygenation over large regions of the global ocean (Bopp et al., 2013; Cocco et al., 2013; Keeling et al., 2010). One potential consequence is the expansion of Oxygen Deficient Zones (ODZs), defined here as waters with suboxic conditions ($[O_2] < 6 \text{ mmol m}^{-3}$). These nitrogen cycle hot spots account for about 30 to 50% of the total fixed N (NO_x, NH₄, and organic N) loss in the ocean, that is, about 70 Tg N yr⁻¹ (Bianchi et al., 2012; DeVries et al., 2012, 2013). This loss occurs through water column denitrification (WCD), whereby we include here both canonical denitrification as well as anaerobic ammonium oxidation (anammox) (Gruber, 2008). Of this loss, 50 to 80% is estimated to occur in the two major ODZs of the Pacific Ocean, i.e., the Eastern Tropical North Pacific (ETNP) and the Eastern Tropical South Pacific (ETSP; Bianchi et al., 2012; Deutsch et al., 2001; DeVries et al., 2012, 2013), regions that experienced a decrease in their oxygen concentration over the past 40 years (Stramma et al., 2008, 2010). Attributing trends in ODZ extents and their associated rates of WCD to anthropogenic forcing is challenging, given the ill constrained variations of dissolved oxygen in the tropical ocean (Frölicher et al., 2009; Long et al., 2016; Rodgers et al., 2015). It is therefore essential to assess the variability of ODZ structures and their associated WCD rates. While many studies have focused on estimating the mean rate of WCD in the Eastern Tropical Pacific (ETP; see Table S1 in the supporting information), only a few have investigated its temporal variability.

These studies suggest that the rates of WCD in the ETP respond quite sensitively to decadal and longer-term climate variability. Using a global ocean biogeochemical model forced with atmospheric data from a reanalysis, Deutsch et al. (2011) reconstructed a strong decrease in the volume of suboxia and the rate of WCD in the ETP between the 1960s and the 1980s. Their model also suggests that these values rebounded in the early 1980s and by around the year 2000, the values were back to the levels of the 1960s. Their results were supported by long-term records of oxygen and nitrate deficits, that is, N* (Gruber & Sarmiento, 1997), in the Southern California Current System, as the signals of this system tend to covary with those of the ETP and because it receives some of its water masses from that region (Castro et al., 2001; Frischknecht et al., 2015).

Further, their simulated decrease in denitrification prior to 1980 and subsequent rapid increase is consistent with the isotopic composition of particulate organic N in sediment core data—a proxy for denitrification—over this period, in the California Current System and in the vicinity of the ETP (Deutsch et al., 2014). Deutsch et al. (2014) further demonstrated that the decrease prior to 1980 is perhaps part of a centennial decreasing trend that only reversed in the 1980s, with the variations largely being driven by changes in tropical wind causing changes in upwelling, productivity, and hence oxygen demand. Further support for a substantial amount of decadal variability in the ETP comes from a recent study by Horak et al. (2016) who analyzed in situ observations of nitrite, N^* , and O_2 in the ETP between 1972 and 2012 and suggested a rapid vertical expansion of suboxia and an increase in denitrification over this period.

While these observations support the existence of large decadal trends in Pacific WCD, they are too sparse in time to determine the magnitude of interannual variability. Nevertheless, variability on this timescale could be quite large given the high variability of the two most important controls of WCD, that is, net primary production (NPP) and dissolved oxygen, in response to the El Niño–Southern Oscillation (ENSO) phenomenon in the ETP (Chavez, Collins, et al., 2002; Fuenzalida et al., 2009; Graco et al., 2016; Stramma et al., 2016). Changes in tropical winds alter the upper ocean distribution of density, oxygen, and nutrients either directly through their effect on upwelling or indirectly through their inducing of equatorial Kelvin waves that change the upper ocean composition across most of the ETP (Belmadani et al., 2012; Chavez, Pennington, et al., 2002; Frischknecht et al., 2015; Hermann et al., 2009). In response to an El Niño, the tropical wind changes cause the isopycnals as well as the isopleths of oxygen and nutrients to be depressed, increasing the oxygen inventory across most of the upper ocean in the ETP, while decreasing the nutrient inventory, curtailing the supply of nutrients to the surface, and lowering primary and export production (the response to La Niña conditions being close to opposite) (Chavez, Collins, et al., 2002; Deutsch et al., 2011; Fuenzalida et al., 2009; Graco et al., 2016; Stramma et al., 2016). While these main threads are well understood, the role of changes in circulation in controlling the O_2 distribution across the upper thermocline is neither well understood nor well quantified. Nevertheless, the observed impact of ENSO on oxygen supply paths and the depth of the oxycline (hypoxic-suboxic boundary) of ODZs (Chavez, Collins, et al., 2002; Fuenzalida et al., 2009) suggest a strong potential to modulate WCD (Deutsch et al., 2011). To date, only the modeling study by Deutsch et al. (2011) showed how ENSO impacts water column denitrification in the ETP, but as the focus of their analyses was the decadal timescale, they did not analyze the ENSO response in detail. Nevertheless, the inspection of their results reveals that their simulated denitrification rates in the ETNP responded strongly to ENSO with maximum and minimum rates attained during La Niña and El Niño phases, respectively.

Here we use a global ocean biogeochemical model forced with reconstructed atmospheric fields to investigate the impact of ENSO variability of Pacific WCD rates. We show that in both ODZs of the ETP wind forcing associated with ENSO drives changes in ocean circulation that lead to very large variations in WCD through a cascade of amplifying effects involving changes in ODZ structure and export production. We further deconstruct the role of solubility, biology, and ocean circulation in driving these changes in ODZ structure.

2. Model and Simulations

2.1. Model

The basis for our study is a slightly modified version of the ocean component (POP2) of the Community Earth System Model v1.2 (CESM), which itself builds on the Community Climate System Model 4 (CCSM4; Gent et al., 2011; Danabasoglu et al., 2011). The ocean component of CESM was run in hindcast mode with a zonal resolution of 1.125° and a meridional resolution varying from 0.53° in the extratropics to 0.27° near the equator. This version of the model includes an anisotropic formulation of viscosity (Jochum et al., 2008) that allows for a better representation of equatorial and high-latitude boundary currents. One important modification in our setup relative to the standard version of POP2 is the imposition of a high isopycnal mixing coefficient of $5 \times 10^8 \text{ cm}^2 \text{ s}^{-1}$ in a small band along the equator (5°S to 5°N , $\sim 259 \text{ m}$ to $\sim 2530 \text{ m}$ depth) to mimic the effect of unresolved equatorial jets that bring oxygenated waters from the west to the ODZs in the east (Getzlaff & Dietze, 2013). This modification substantially decreases the bias in the modeled oxygen distribution in the ETP (see below).

Embedded in the CESM ocean component is the Biological Elemental Cycling (BEC) model, a marine plankton functional type model (Moore et al., 2004, 2013). It simulates the biogeochemical cycling of most major elements in the ocean (C, N, P, O, Si, and Fe) and includes three explicit phytoplankton types, one implicit calcifier as well as an adaptive zooplankton group. The latter routes grazed material to the inorganic,

dissolved organic, and particulate organic pools depending on the prey type. Dissolved organic matter is split into a semilabile and refractory pool, and each of these pools is remineralized following an element-specific constant rate of remineralization. Particulate organic matter dynamics are represented implicitly by distributing remineralization throughout the water column upon production, following an exponential curve with a variable length scale. The particulate organic matter remineralization rate is reduced at concentrations of $[O_2] < 35 \text{ mmol m}^{-3}$. This is achieved by multiplying the remineralization length scale by a factor whose value increases linearly from 1 at $[O_2] = 35 \text{ mmol m}^{-3}$ to a maximum of 3 when $[O_2] \leq 5 \text{ mmol m}^{-3}$.

The employed version of BEC incorporates all the major processes of the marine N cycle. Fixed N enters the ocean through marine N_2 fixation, atmospheric deposition, and riverine inputs; fixed N is removed via denitrification in the water column and the sediments as well as via burial. Concretely, water column denitrification is parameterized to set in at an oxygen threshold $O_2^{\text{onset}} = 7 \text{ mmol m}^{-3}$ and is then assumed to increase linearly with respect to decreasing $[O_2]$ to its maximum rate at $O_2^{\text{full}} = 5 \text{ mmol m}^{-3}$. This maximum rate is computed by multiplying the organic carbon remineralization rate, $J_{\text{remin}}(\mathbf{x}, t)$ with a conversion efficiency of $R_{N:C}$ (moles of NO_3^- consumed per moles of organic carbon), assumed to be 112:117 (Paulmier et al., 2009). This gives for WCD

$$J_{\text{WCD}}(\mathbf{x}, t) = R_{N:C} \cdot H(O_2(\mathbf{x}, t)) \cdot J_{\text{remin}}(\mathbf{x}, t), \quad (1)$$

where

$$H(O_2(\mathbf{x}, t)) = \begin{cases} 1, & \text{if } O_2(\mathbf{x}, t) < O_2^{\text{full}} \\ \frac{O_2^{\text{onset}} - O_2(\mathbf{x}, t)}{O_2^{\text{onset}} - O_2^{\text{full}}}, & \text{if } O_2^{\text{onset}} \leq O_2(\mathbf{x}, t) \leq O_2^{\text{full}} \\ 0, & \text{if } O_2(\mathbf{x}, t) > O_2^{\text{onset}} \end{cases}$$

A description of the full N cycle in CESM-BEC can be found in Yang and Gruber (2016).

2.2. Simulations

We run the ocean component of CESM with its embedded BEC model from 1948 to 2009 in hindcast mode, using the interannually varying atmospheric forcing data set of Large and Yeager (2009). The N inputs via atmospheric deposition and rivers are kept constant at their preindustrial levels throughout the simulations. The initial conditions for this production run were provided by spinning up the model for four forcing cycles (62 years each), following the Core-II protocol of Griffies et al. (2011). The production run thus represents the fifth cycle. To calculate model drift, we run one additional forcing cycle, bringing the total number of cycles to six. The model drift was calculated by a running mean over the fifth cycle with a window size of a full cycle (62 years) for each variable of interest at each grid point. The results shown come from the last 50 years of the production run (fifth cycle, 1960–2009) and are corrected for the drift. Although not negligible, the drift is small relative to the signals we are reporting and discussing here. For example, the drift in global WCD over the simulated period amounts to $\sim 0.05 \text{ Tg yr}^{-1} \text{ yr}^{-1}$, which is substantially smaller than the simulated ENSO-driven fluctuations frequently reaching values of over 20 Tg yr^{-1} (see section 4.1).

2.3. Model Evaluation

The successful modeling of the variability of water column denitrification in the ETP in response to ENSO and other climate variability patterns requires the model (i) to capture the observed changes in temperature, circulation, and mixing; (ii) to reasonably represent the distribution of oxygen in the ETP, especially the extent of the ODZs; and (iii) to simulate the distribution and magnitude of primary and export production. We evaluate these three elements in turn.

Our hindcast simulation successfully captures the main climate variability patterns over the Pacific observed over the last few decades, especially those associated with ENSO. Namely, the model reproduces the temporal variations of the observed sea surface temperature (SST) anomalies over the Niño 3.4 region ($0-10^\circ\text{S}$, $90^\circ\text{W}-80^\circ\text{S}$; $R^2 = 0.83$; Figure 1a), one of the key characteristics of ENSO. It also reproduces well the observed spatial pattern of the anomalies of SST ($R^2 = 0.94$) and sea surface height (SSH; $R^2 = 0.87$) averaged over all ENSO events (Figures 1b–1e). The model's principal component associated with the first leading empirical orthogonal function (EOF) of SST anomalies over the North Pacific (poleward of 20°N) also agrees very well with that based on observations, reflecting the Pacific Decadal Oscillation ($R^2 = 0.83$, Figure S2). Finally, our simulation also captures the second EOF of SST over the same region ($R^2 = 0.76$, Figure S2), associated with

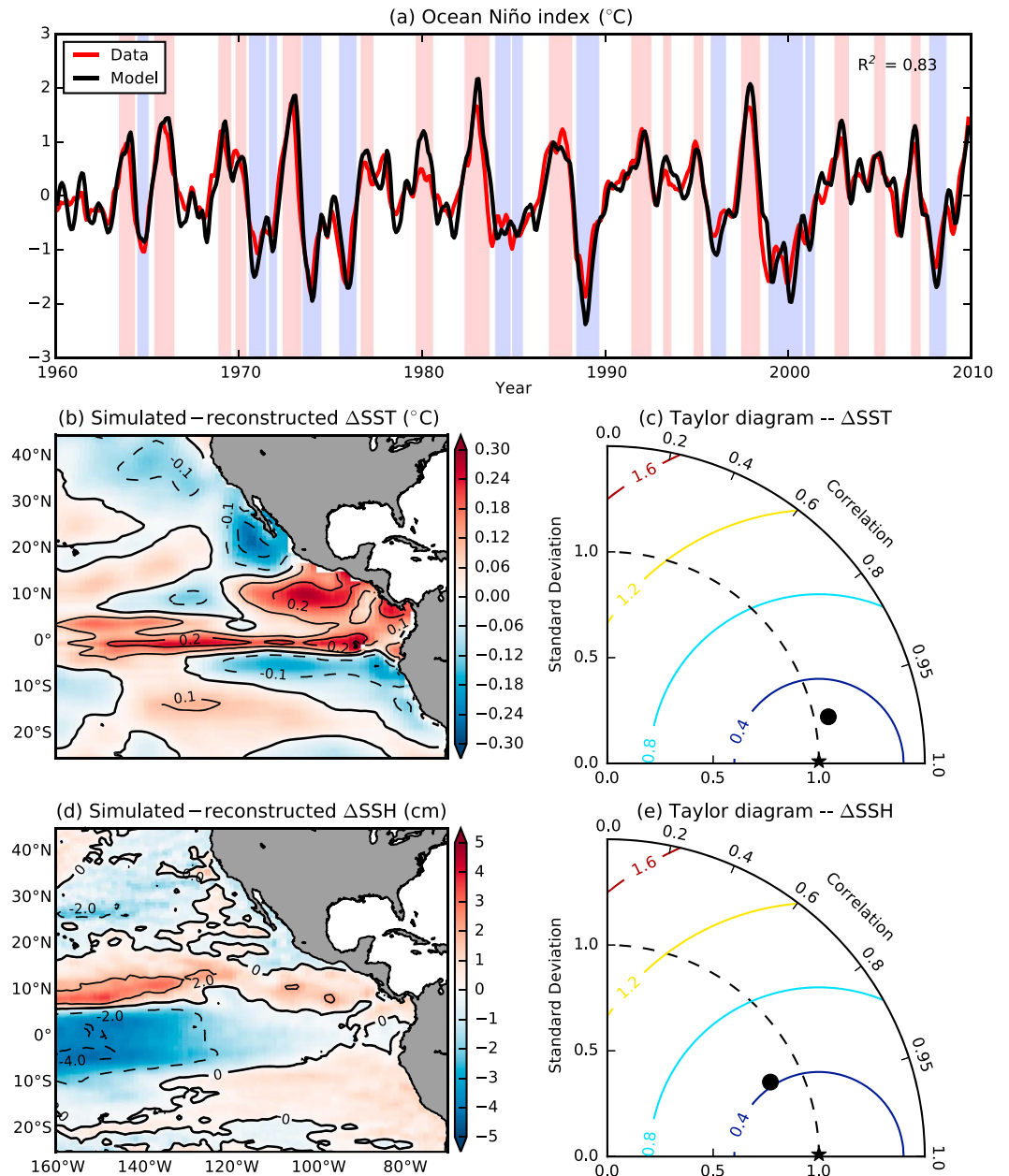


Figure 1. Simulated versus observed ENSO variability in the Pacific Ocean. (a) Simulated (black curve) versus observed (red curve) corrected Ocean Niño index (cONI) calculated as the three-monthly running mean of the detrended sea surface temperature (SST) anomalies in the Niño 3.4 region (5°S–5°N, 170°W–120°W) in °C. Red shadings indicate El Niño events, and blue shadings indicate La Niña events following the definition described in section 3.1. (b) Simulated minus reconstructed SST anomalies for the average ENSO event in °C. (c) Taylor diagram of simulated and reconstructed SST anomalies for the average ENSO event in the Pacific Ocean. (d) Same as Figure 1b but for sea surface height (SSH) anomalies. (e) Same as Figure 1c but for sea surface height (SSH) anomalies. The SST data stem from the Extended Reconstructed SST version 4 (Huang et al., 2014), and the SSH data stem from the Ocean Reanalysis System 4 (Balmaseda et al., 2013).

the variability of the North Pacific gyre circulation, which has been shown to be highly correlated with surface nitrate and chlorophyll in the northeastern Pacific Ocean (Di Lorenzo et al., 2008).

Current global Earth System Models are known to poorly reproduce the positioning and size of the ODZs in the Eastern Tropical Pacific (Cabre et al., 2015). These models especially tend to overestimate the extent of suboxia at the equator, leading to the merging of the ODZs of the ETNP and ETSP into one. In our configuration

of CESM, we addressed this issue by enhancing the equatorial mixing, mimicking unresolved jets that bring oxygenated waters toward the ODZs in the eastern Pacific (Figure S1). This, together with the consideration of reduced rates of remineralization in the ODZ (section 2.1), assisted in bringing the simulated structures of the ODZs closer to the observations.

This is particularly the case for the upper portions of the ODZs (above 500 m depth) where both the latitudinal extents and thicknesses of the modeled north and south Pacific ODZs closely match those calculated from World Ocean Atlas data (Bianchi et al., 2012; Figures 2a and 2b). At depth, however, the simulated O_2 is too low in the ETNP resulting in the core of its ODZ to be too thick and its boundary to extend too far north (Figure 2c). As a result, the mean simulated volume of the northern ODZ is biased high, close to double that calculated from observations (Figures 2a and 2e). In the ETSP, however, when accounting for its variability, the simulated mean volume of the ODZ is indistinguishable from observational estimates, though its lateral spatial extent appears to be more confined to the coast as compared to observations (Figures 2b, 2d, and 2f).

We simulate an average WCD rate integrated over the ETP of 71 Tg N yr^{-1} for the period of 1960 through 2009. This rate is at the high end of current estimates that range from 39 to 63 Tg N yr^{-1} (Table S1). This stems primarily from the simulated WCD in the ETNP being substantially larger than current estimates suggest (Table S1), that is, 52 Tg N yr^{-1} versus 19 to 29 Tg N yr^{-1} in recent observations. This positive bias is consistent with the overestimation of the simulated volume of the ODZ in that region (Figures 2c and 2e). The simulated WCD rates in the ETSP are within the range of estimates (19 Tg N yr^{-1} versus 18 to 30 Tg N yr^{-1} in the most recent estimates; Table S1).

The simulated patterns of net primary production and export compare overall favorably to observationally based estimates. However, coastal productivity is simulated to be too low in the model (Figures S3b and S4b). This is likely attributable in part to the poor representation of coastal dynamics at the relatively coarse resolution we employ here, apparent from the inability of the model to reproduce near surface coastal currents (Figure S5). Despite this bias, the model captures the increase in NPP and export following the 1998 El Niño in the upwelling regions of the Eastern Pacific although with a lower amplitude than the increase inferred from satellite data (Figures S3d, S3e, S4d, and S4e).

Overall, despite some shortcomings, we consider this model to be well positioned to assess and analyze interannual to decadal variability in WCD and ODZ dynamics in the ETP. Of particular note is the improved representation of the oxygen distribution in our model, particularly in the low oxygen regions of the Eastern Tropical Pacific (Figures 2 and S1).

3. Analysis Framework

3.1. Composite Analysis

In order to analyze the impact of ENSO variability on WCD and ODZ extent, we build a composite of the anomaly fields from all El Niño and La Niña events to form a canonical mean response (Deser et al., 2012). We thereby reverse the sign of anomalies for La Niña, as the response of ocean circulation and tracer distributions are close to symmetric with respect to the sign of the Niño 3.4 index, i.e., the SST anomalies of the Eastern Tropical Pacific in the Niño 3.4 region. Thus, all responses are reported relative to a positive phase of ENSO, that is, an El Niño episode.

To identify ENSO events, we use the corrected Oceanic Niño Index (cONI), defined as the three monthly running mean of the detrended Niño 3.4 index. We detrend the latter index by removing a fourth-order polynomial fit. This ensures the removal of not only a long-term linear trend but also of variations on decadal and interdecadal timescales that can mask some of the ENSO-related variations. El Niño and La Niña events are then defined as periods of at least five consecutive months when the cONI is larger than 0.5°C or smaller than -0.5°C , respectively. This resulted in the identification of a total of 16 El Niño events and 12 La Niña events over the 1960 through 2009 period.

When computing composites from the deseasonalized fields, we again removed decadal or longer scale variability by fitting a fourth-order polynomial at each ocean grid point over the period of 1960 through 2009. The detrended field is then averaged over all months qualifying as either an El Niño or a La Niña event. We also build a 24 monthly-stacked composite of all ENSO events in order to analyze their mean temporal evolution.

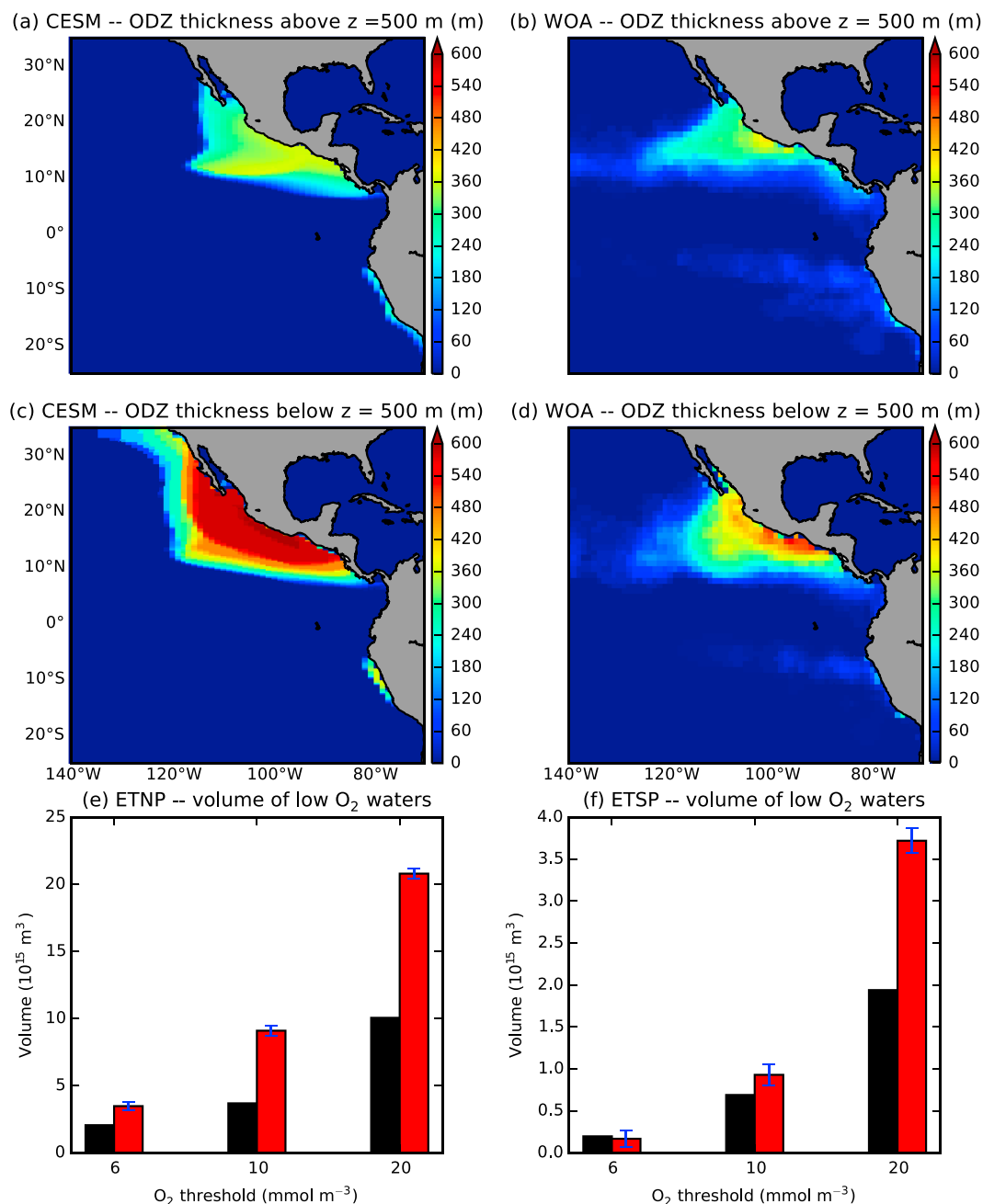


Figure 2. Simulated versus observed ODZ thickness and volumes. (a) Simulated ODZ ($O_2 < 6 \text{ mmol m}^{-3}$) thickness above a depth of 500 m averaged over the period from 1960 to 2009 in meters. (b) Same as Figure 2a but for the corrected World Ocean Atlas data (Bianchi et al., 2012). (c) Same as Figure 2a but calculated for waters that are below a depth of 500 m. (d) Same as Figure 2b but calculated for waters that are below a depth of 500 m. (e) Simulated versus observed volumes of water for various O_2 threshold in the ETNP averaged over the period from 1960 to 2009. (f) As in Figure 2c but in the ETSP. The error bars represent one standard deviation of the simulated volumes over the same period.

To do so, we select the 12 months preceding and following the January 1st closest to the Niño 3.4 peak and average over individual months.

3.2. Separation of the Drivers for Water Column Denitrification

The total WCD rate within an ODZ is determined by the organic matter remineralization field, $J_{\text{remin}}(\mathbf{x}, t)$, and the geometry of the ODZs. Thus, a change in WCD can result from any combination of these two main factors. We present here a framework that enables their separation.

Using (1), the WCD integrated over any volume V is given by

$$\int J_{\text{WCD}}(\mathbf{x}, t) dV = R_{\text{N:C}} \int H(\text{O}_2(\mathbf{x}, t)) J_{\text{remin}}(\mathbf{x}, t) dV. \quad (2)$$

Concretely, WCD can vary either via $H(\text{O}_2(\mathbf{x}, t))$, that is, due to changes in the O_2 distribution that determine the volume over which denitrification is occurring, or via $J_{\text{remin}}(\mathbf{x}, t)$, that is, the rate of organic matter remineralization. We can separate their relative contribution to the variations in WCD by using a Reynolds-like decomposition, expressing quantities as the sum of mean (bar) and anomaly (prime) components. Using $H = \bar{H} + H'$ and $J = \bar{J}_{\text{remin}} + J'_{\text{remin}}$ in equation (2) gives

$$\int J_{\text{WCD}}(\mathbf{x}, t) dV = R_{\text{N:C}} \int (\bar{H} + H') (\bar{J}_{\text{remin}} + J'_{\text{remin}}) dV, \quad (3)$$

where we omitted the arguments of H and J for simplicity. Multiplying out the right-hand side and rearranging the terms gives an expression for anomalies in integrated WCD:

$$\begin{aligned} \int J_{\text{WCD}}(\mathbf{x}, t) dV - R_{\text{N:C}} \int (\bar{H} \cdot \bar{J}_{\text{remin}}) &= R_{\text{N:C}} \int (H' \cdot \bar{J}_{\text{remin}}) dV \\ &\quad \underbrace{\hspace{10em}}_{\text{mean } J_{\text{WCD}}} \quad \underbrace{\hspace{10em}}_{\Delta J_{\text{WCD}} \text{ driven by } \text{O}_2 \text{ changes}} \\ &\quad + R_{\text{N:C}} \int (\bar{H} \cdot J'_{\text{remin}}) dV \\ &\quad \underbrace{\hspace{10em}}_{\Delta J_{\text{WCD}} \text{ driven by remin. changes}} \\ &\quad + R_{\text{N:C}} \int (H' \cdot J'_{\text{remin}}) dV \\ &\quad \underbrace{\hspace{10em}}_{\Delta J_{\text{WCD}} \text{ driven by covariation}} \end{aligned} \quad (4)$$

3.3. Potential Drivers for Changes in Dissolved O_2

In the upper ocean near the surface, the oxygen concentration is kept close to its saturation value (O_2^{sat}) owing to the combined action of rapid air-sea gas exchange and biological production (Ito et al., 2004; Sarmiento & Gruber, 2006). Upon detrainment from the upper ocean mixed layer, and especially once the water is transported away from the euphotic zone, the remineralization of organic matter reduces its oxygen content along its path. The Apparent Oxygen Utilization (AOU), defined as the difference between the oxygen concentration of a water parcel at saturation and its actual oxygen concentration,

$$\text{AOU}(\mathbf{x}, t) = \text{O}_2^{\text{sat}}(\mathbf{x}, t) - \text{O}_2(\mathbf{x}, t), \quad (5)$$

is then a good measure of the degree of consumption of oxygen that has occurred since the water parcel's last contact with the atmosphere. We recognize that O_2^{sat} is only an approximate estimate for the preformed value of O_2 , as many processes, including bubble mediated gas transfer, biological production, physical mixing, and incomplete equilibration (Hamme & Emerson, 2006; Hamme & Severinghaus, 2007), can lead to deviations of the preformed O_2 from O_2^{sat} (Ito et al., 2004). However, for the purpose of our analyses here, these deviations are not critical, particularly since we focus on temporal changes for which variations in the preformed oxygen are small (<5%) compared to the analyzed O_2 signals (Figure S6). Under this assumption ($\text{O}_2^{\text{sat}} \sim$ preformed oxygen), the AOU of a water parcel is a good measure of the oxygen utilization rate (J_{OUR}) along its path over the time τ since it left contact with the atmosphere, that is,

$$\text{AOU} = \int_0^\tau J_{\text{OUR}} d\tau, \quad (6)$$

where we assumed that preformed AOU is zero, and where we omitted, as above, the arguments for simplicity. J_{OUR} is mechanistically tied to the rate of remineralization of organic matter, J_{remin} , along the path of the water parcel such that

$$J_{\text{OUR}} = (1 - H(\text{O}_2)) \cdot J_{\text{remin}} \cdot R_{\text{O}_2:\text{C}}, \quad (7)$$

where we took into account only the fraction of the remineralization that occurs by using O_2 as oxidant ($1 - H(O_2)$) and converted the rate from carbon to oxygen units via the stoichiometric ratio $R_{O_2:C}$.

Given (6), the mean J_{OUR} along the path of the parcel is given by the ratio of AOU and τ , i.e.,

$$\bar{J}_{OUR} = \frac{\int_0^\tau J_{OUR} d\tau}{\int_0^\tau d\tau} = \frac{AOU}{\tau}. \quad (8)$$

Using a Reynolds-like decomposition of J_{OUR} and the transit time τ ($J_{OUR} = \bar{J}_{OUR} + J'_{OUR}$ and $\tau = \bar{\tau} + \tau'$) gives after some rearrangement an expression for the anomalies in AOU (AOU'):

$$AOU' = AOU - \overline{AOU} = \underbrace{\int_{\bar{\tau}}^{\bar{\tau}+\tau'} \bar{J}_{OUR} d\tau}_{\text{circulation driven}} + \underbrace{\int_0^{\bar{\tau}} J'_{OUR} d\tau}_{\text{OUR driven}} + \underbrace{\int_{\bar{\tau}}^{\bar{\tau}+\tau'} J'_{OUR} d\tau}_{\text{covariance driven}}, \quad (9)$$

where analogous to the decomposition of the WCD variations, we can identify a term associated with changes in circulation (evidenced by anomalies in τ), a term associated with changes in J_{OUR} , and a term associated with the covariation between J_{OUR} and circulation/mixing.

In order to fully evaluate the integrals in (9), one would have to undertake a Lagrangian analysis, which we consider to be beyond the scope of our study. To identify the main drivers of the changes in AOU without the need to fully quantify them, we simplify the above by making the assumption that the variations along the flow path are spatially homogeneous. In this case, the arguments of the integrals become constant, and (9) simplifies to

$$AOU' \approx \underbrace{\tau' \cdot \bar{J}_{OUR}}_{\text{circulation driven}} + \underbrace{\bar{\tau} \cdot J'_{OUR}}_{\text{OUR driven}} + \underbrace{\tau' \cdot J'_{OUR}}_{\text{covariance driven}}. \quad (10)$$

We will be using this simplified analysis, recognizing that it is an approximation. However, since the changes of interest here tend to have tropical Pacific-wide anomaly patterns, we deem our approximation to be of sufficient accuracy for our purposes. To reflect this approximation, we only analyze spatially integrated anomalies over the entire Eastern Tropical Pacific. Given the Lagrangian nature of our analysis, we do this integration along isopycnals.

4. Results and Discussion

4.1. Simulated Variability: WCD and ODZ Structure

We simulate large variations of WCD rates in the Eastern Tropical Pacific that are tightly linked to ENSO variations (Figures 3a and 3c). In fact, 63% of the detrended variations in WCD rates can be explained by variations in the corrected Oceanic Niño Index (cONI; section 3.1). In particular, El Niño episodes are associated with low WCD rates relative to the mean, and vice versa during La Niña episodes. The average response of WCD to ENSO is of roughly equal magnitude in both the ETNP and ETSP, respectively, yielding a change of about $\pm 13 \text{ Tg yr}^{-1}$ averaged over the mean ENSO episode. This corresponds to a variation of about $\pm 20\%$ of the mean rate. The peak-to-peak fluctuations between an El Niño and a La Niña event are even more compelling with variations of over $\pm 70\%$ of the mean rate (Figures 3a and 3c).

In the ETNP, the depth-integrated changes in WCD are largest in the southern portion of the ODZ ($\sim 10^\circ\text{N}$), off the coast of central America (Figure 4a). In contrast, they are more homogeneously distributed in the ETSP (Figure 4a). Composites of horizontally integrated denitrification rates as a function of depth reveal the largest changes in WCD to occur in the upper part of the ODZs (Figures 5a–5d). More specifically, 50% of the total change in denitrification in the ETNP occurs within the top portion of the ODZ over a volume corresponding to only 11% of the total mean ETNP ODZ volume. In the ETSP, this is even more extreme, with 50% of the change in the denitrification in the ETSP occurring over a volume corresponding to only 5% of the mean ODZ volume in that region. Although our focus here is on the mean response of WCD to ENSO, we also analyzed the response to individual events (Figures S7a and S7b, note that the sign is such that the signal is shown for an El Niño episode). Although there is indeed some variations between individual events—as is the case for many physical properties (e.g., Capotondi et al., 2015)—the average response of WCD is a robust representation of most individual events. The outliers tend to correspond to periods with low SST anomalies

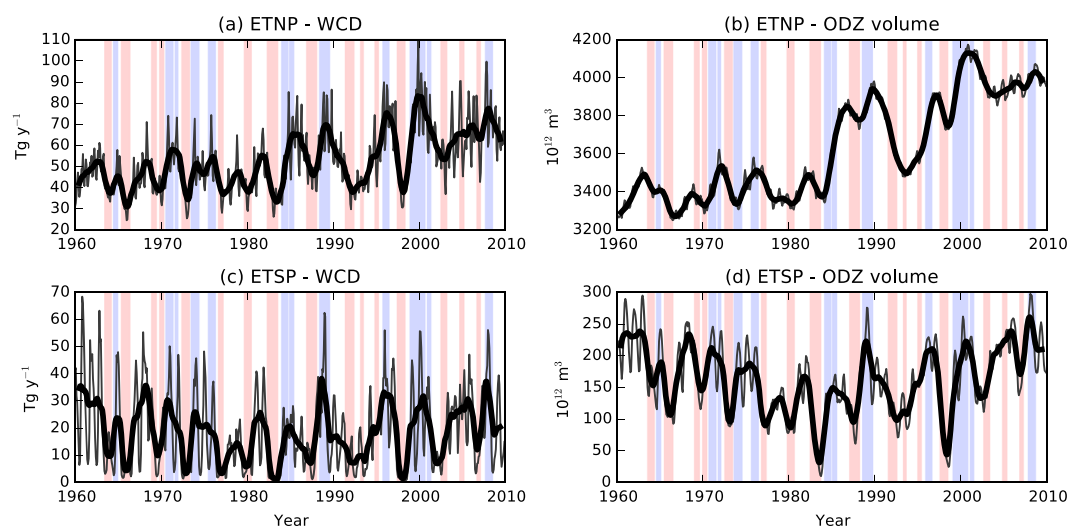


Figure 3. Time evolution of simulated volume-integrated water column denitrification rate (WCD) and ODZ volume. (a) WCD integrated over the North Pacific ODZ. (b) North Pacific ODZ volume ($[O_2] < 6 \text{ mmol m}^{-3}$). (c) As in Figure 3a but for the South Pacific ODZ. (d) As in Figure 3b but for the South Pacific ODZ. Thick lines show the 12 months running means, while the thin ones show the monthly averaged values. Red shadings indicate El Niño events, and blue shadings indicate La Niña events following the definition described in section 3.1.

over the Niño 1,2 region in the very Eastern Tropical Pacific ($0-10^\circ\text{S}$, $90^\circ\text{W}-80^\circ\text{S}$). This suggests that while our analysis is very representative, caution must be taken when applying the canonical response to any individual ENSO events, particularly those that have a more central Pacific flavor.

The total volume of the two ODZs in the ETP also responds to ENSO, with a correlation of the detrended ODZ volume variation with changes in the cONI of $R^2 = 27\%$ at a lag of 3 months. But the relative changes are much smaller than those for WCD. Averaged over all events and integrated over both ODZs, their volume changes by only about $\pm 2\%$ with a smaller volume change during El Niño episodes. However, there are large differences between the two ODZs. In the ETNP, the volume change is actually less than $\pm 2\%$, while in the ETSP it is more than $\pm 25\%$. The reason for the total change in ODZ volume being dominated by those of the ETNP is due to the fact that its volume is about 22 times larger than that of the ETSP.

Hidden behind the small change in the overall ODZ volume of the ETNP are much larger local changes that tend to compensate each other (Figures 4b and 5e), for example, the ODZ volume of the ETNP decreases above 400 m while it increases below. This contrasts with the ETSP, where the change in the ODZ volume is of the same sign throughout the water column, with a larger fraction of the perturbation concentrated in the upper water column, that is, above 350 m (Figure 5f). Both ODZs also exhibit large variations of the depth of their upper boundary (defined here as the 6 mmol m^{-3} isopleth of O_2) in response to ENSO variability. The ENSO response of this upper boundary, which we subsequently refer to as the oxycline, is also spatially variable in the ETNP, with the largest changes in oxycline depth ($>40 \text{ m}$) occurring in the southeastern sector of the ODZ (Figure 4c). The changes in the South Pacific oxycline depth are spatially homogeneous with an average change of over 100 m (Figure 4c). This is consistent with the spatially relatively homogeneous changes of the ODZ thickness in the ETSP and strong spatial variations in the ETNP (Figure 4b).

The export of organic matter in the ETP and especially above its ODZs also exhibits consistent variations in response to ENSO (Figure 4d, $R^2 = 65\%$), with El Niño episodes leading to a 6% reduction in the export flux integrated over the climatological maximum extent of the ODZs. The largest variations in the export flux occur over the ODZs and over the equatorial cold tongue with local changes exceeding 25% of the mean flux (Figure 4d).

Taken together, the decrease in WCD during El Niño episodes is a consequence of a combination of a higher degree of oxygenation in the upper waters of the ETP and lower export production creating a lower demand for oxidants. The model simulations also demonstrate that during La Niña episodes, the same processes are at play but acting in opposite directions. Thus, while the processes governing the changes in WCD are well understood, it is not straightforward to explain how the relatively small changes of the ODZ volumes ($\pm 2\%$)

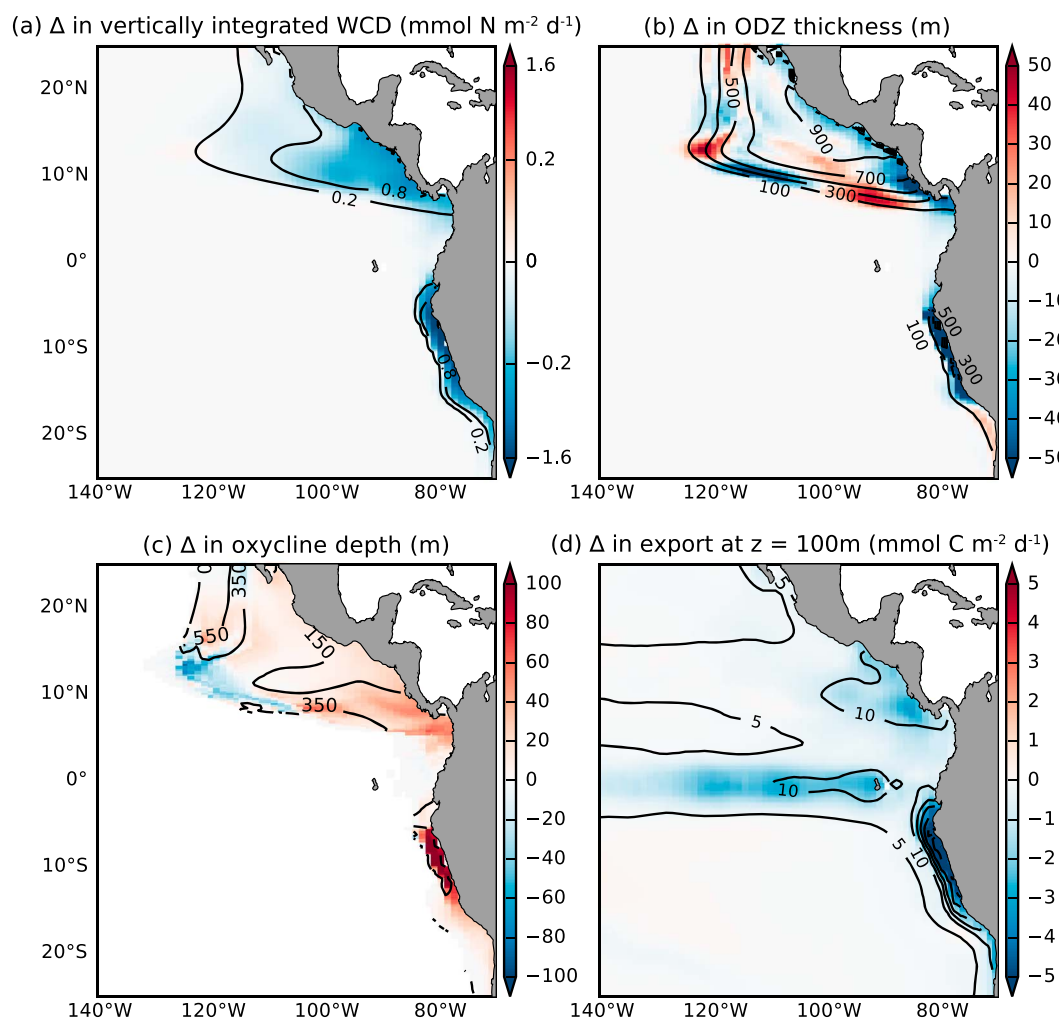


Figure 4. Maps of ENSO-composited changes. (a) Change in the vertically integrated rate of water column denitrification (WCD) in $\text{mmol m}^{-2} \text{d}^{-1}$. (b) Change in ODZ thickness in meter ($[\text{O}_2] < 6 \text{ mmol m}^{-3}$). (c) Change in the depth of the upper oxycline in meter ($\text{O}_2 = 6 \text{ mmol m}^{-3}$ isopleth). (d) Change in carbon export at a depth of 100 m in $\text{mmol C m}^{-2} \text{d}^{-1}$. Contours in each panel indicate the mean state. Note the logarithmic color scale for WCD in Figure 4a.

and those of the export of organic matter over the ODZ extent ($\pm 6\%$) can explain the relatively large responses of the total Pacific WCD ($\pm 20\%$). Is this amplification a consequence of the threshold behavior of WCD with regard to oxygen, or are other processes of importance as well? In the following, we will disentangle and quantify these contributions, building on the analysis framework established in section 3.2.

4.2. Drivers of WCD Variability

We decomposed the horizontally integrated WCD anomalies (Figures 5c and 5d) into a component driven by ODZ geometry alone (red lines), by carbon remineralization alone (green line), and by their covariation (blue line; see equation (4) in section 3.2). Spatially integrated over the ETNP, the ENSO-driven changes in oxygen and organic matter remineralization contribute equally ($\sim 50\%$) to the response of WCD with the covariation term (blue line) being very small in comparison. In contrast, the changes in WCD integrated over the ETSP are primarily driven by variations in ODZ structure, with 94% of the change attributable to this process. The contribution of carbon remineralization ($+15\%$) and of the covariation (-9%) is small in comparison.

Thus, the vertical positioning of the ODZ relative to the rates of remineralization appears to be a very critical component of the answer to our amplification puzzle. This is because a given change in ODZ volume does not contribute equally to changes in denitrification at every depth, as this critically depends on the magnitude

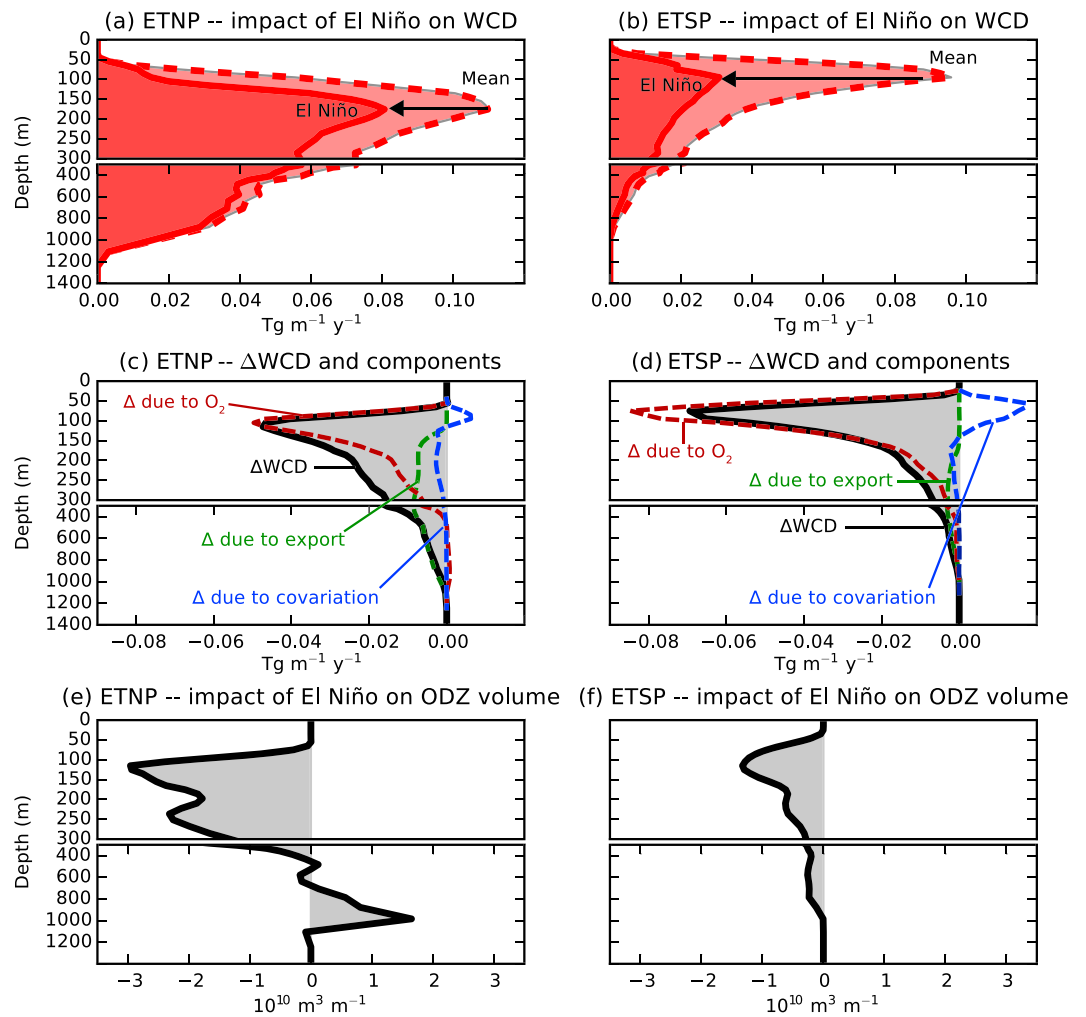


Figure 5. Vertical profiles of ENSO-composited changes. (a) Mean state and ENSO-perturbed horizontally integrated WCD over the ETNP in $\text{Tg N m}^{-1} \text{yr}^{-1}$. Dashed lines show the mean state and solid lines the ENSO-perturbed state. (b) As for Figure 5a but for the ETSP. (c) WCD anomalies horizontally integrated over the ODZ of the ETNP for the average ENSO response (solid black line). Also shown as colored dashed lines are the component changes in WCD as outlined in section 3.2: the red line shows changes due to O_2 only, the green line shows changes due to carbon remineralization only, and the blue line shows changes due to their covariation. (d) As in Figure 5c but for the ODZ of the ETSP. (e) Change in the horizontally summed ODZ volume in the ETNP in $10^{10} \text{ m}^3 \text{ m}^{-1}$. (f) As in Figure 5e but for the ODZ in the ETSP.

of organic matter being subject to remineralization (cf. Deutsch et al., 2011). The largest change in water column denitrification per ODZ volume change occurs in the upper part of the ODZ, because this is where remineralization rates are highest (Figures 5c and 5d). At depth, the smaller remineralization rates require a much larger change in ODZ volume in order to modify total WCD rates substantially. Therefore, it is possible for substantial changes in total WCD to occur with no or little ODZ volume change, for example, by solely displacing the ODZ vertically. This mechanism explains why the variability of WCD in the North Pacific ODZ is much larger than the combined variability of the total ODZ volume and the export of organic matter above it, solving the apparent amplification paradox. But what we have not addressed yet is how ENSO controls the oxygen variations in the ETP. We assess this following the approach outlined in section 3.3.

4.3. Drivers of O₂ Variability

Figure 6a that depicts the regionally integrated O₂ change components as a function of potential density referenced to the surface reveals that the changes in O₂ are largely dominated by changes in AOU (blue line). This is most accentuated above the isopycnal surface $\sigma_0=28.2$, which has a mean depth of about 330 m. But throughout the upper water column, the AOU-driven changes are compensated by changes in solubility (Figure 6a, red line). This compensation occurs because during El Niños, the increase in upper ocean temperature

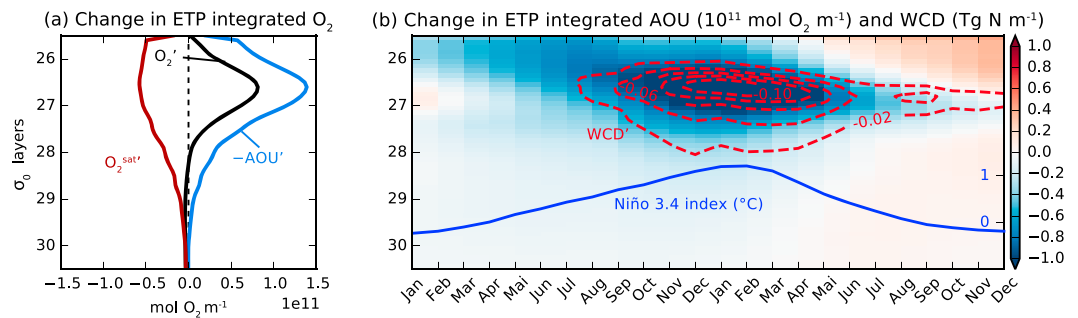


Figure 6. Processes controlling the O_2 distribution and WCD in the ETP. (a) ENSO-composited change in O_2 , AOU, and O_2^{sat} integrated along isopycnals over the Eastern Tropical Pacific. (b) Monthly ENSO-composited evolution of AOU anomalies (color) and WCD (contours) integrated along isopycnals over the Eastern Tropical Pacific. The blue line shows the evolution of the composited Niño3.4 index in $^{\circ}\text{C}$. The ETP integrals were performed over the region bounded by 25°S – 25°N and 140°W – 90°W (see box in Figure 7).

reduces the solubility of O_2 , and vice versa during La Niñas (Ito & Deutsch, 2013). Below $\sigma_0=28.2$, changes in O_2^{sat} become dominant, causing the O_2 inventory to slightly decrease during El Niños, explaining the simulated increase in the northern ODZ volume at depth (Figure 5e).

The anomalous changes in AOU can occur in response to anomalous variations in either the transit time (τ')—the time since the water parcel was last in contact with the atmosphere—or the rate of oxygen consumption (J'_{OUR}) along the path of the water parcel (see section 3.3). During El Niños, both J_{OUR} and τ decrease below $\sigma_0=26.5$, each potentially contributing to the decrease in AOU over the ETP. However, the strong correlations of AOU' and τ' (compare colors and contours in Figure 7b) and the relatively small change in the rates of J_{OUR} (Figure 7a) suggest that changes in ocean circulation and mixing play a more important role in driving the changes in AOU. To confirm this, we use equation (10) in section 3.3 to decompose AOU' into three components, that is, one driven by changes in ocean circulation/mixing, one driven by changes in OUR, and one driven by the covariation of the two changes.

When integrated along isopycnals over the ETP, we find that changes in the circulation component (red line) drive most of the ENSO-related anomalies in AOU (black line) depicted in Figure 7d. In contrast, the changes due to anomalies in OUR (green line) in fact reduce AOU' (or increase O_2) over most of the water column, except between $\sigma_0 = 26.5$ and $\sigma_0 = 27.0$ where its contribution remains small (<10%). The contribution of the covariance term (blue line) is negligible throughout the water column (Figure 7d). Given that we used an approximation to separate out the different components driving changes in anomalous AOU, we also need to look at other, independent ways to confirm our conclusion.

We further confirm the leading role of ocean circulation and mixing in driving the anomalies in AOU' by estimating the isopycnal inventory change in AOU caused by variations in the local rates of O_2 utilization. This is achieved by integrating the local rates of O_2 utilization along isopycnal over the ETP, after having multiplied them by the average length of an ENSO event ($J'_{\text{OUR}} \cdot \Delta t_{\text{ENSO}}$; Figures 7a and 7c). On isopycnals shallower than $\sigma_0=26.5$, the O_2 inventory changes from $J'_{\text{OUR}} \cdot \Delta t_{\text{ENSO}}$ are opposite of those observed in AOU' . Below $\sigma_0=26.5$ down to $\sigma_0=28.5$, where the largest changes in denitrification occur (Figure 6b, contours), $J'_{\text{OUR}} \cdot \Delta t_{\text{ENSO}}$ can only contribute between 8 and 16% of the inventory change in AOU' . The above analysis thus confirms our initial assertion that the response of AOU is primarily driven by changes in ocean circulation and mixing.

To better understand how changes in ocean circulation and mixing alter the oxygen distribution on isopycnals, we investigate next the monthly time evolution AOU and the ocean currents on $\sigma=26.8$ (Figures 8b–8h), that is, the isopycnal where the largest changes in AOU (and WCD) are simulated (see Figure 8a for the mean state). As was already evident from Figure 6b, the progression of the anomalies in AOU and WCD through time can be viewed as a two-phase process, that is, a buildup phase as the ENSO episode is developing toward its peak at the end of the calendar year, followed by a decay phase.

During the buildup phase (Figures 8b–8e), the trade winds tend to strengthen east of 120°W (Figure S8). This causes the Equatorial Counter Current (ECC) to strengthen in this region (Montes et al., 2010), causing anomalous AOU to accumulate eastward (Figures 8b–8f). Additionally, a meridional increase in the wind stress curl gradient (Figure S8) causes the North Equatorial Counter Current and the Peru-Chile Counter Current

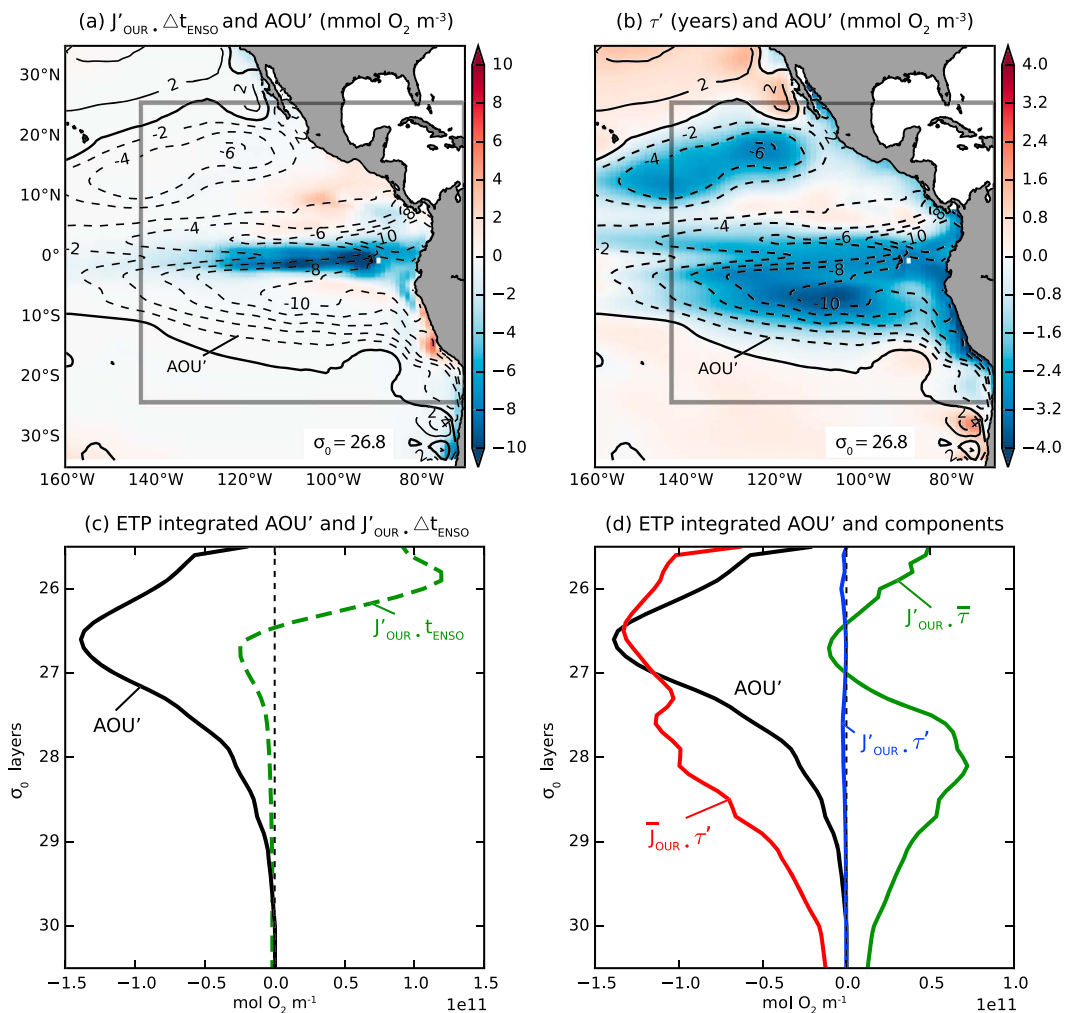


Figure 7. Analysis of the processes contributing to the ENSO-related anomalies in AOU. (a) Change in O_2 consumption multiplied by the average length of an ENSO event ($J_{OUR} \times \Delta t_{ENSO}$, color map) and anomaly in AOU (AOU' , contours) on the isopycnal $\sigma_0=26.8$ in $mmol O_2 m^{-3}$. (b) As in Figure 7a but for anomalies in transit time (τ' , color map) in years together with AOU' (contours). (c) Anomalies in AOU (AOU' ; black line) and O_2 consumption multiplied by the average length of an ENSO event ($J_{OUR} \times \Delta t_{ENSO}$, dashed green line) integrated along isopycnals over the Tropical Pacific in $mol O_2 m^{-1}$. (d) Change in AOU (AOU' ; black line) decomposed into components (dashed lines) as outlined in section 3.3 integrated along isopycnals over the Tropical Pacific in $mol O_2 m^{-1}$. The red line shows changes due to circulation/mixing only, the green line due to changes in OUR only, and the blue line due to their covariation. The data in Figures 7c and 7d were averaged over the gray box in Figures 7a and 7b, that is, spanning the region bounded by $25^{\circ}S-25^{\circ}N$ and $140^{\circ}W-90^{\circ}W$.

(Chaigneau et al., 2013; Montes et al., 2010), two currents that supply the ODZs with low AOU (high O_2) waters, to strengthen (see also Chen et al., 2016). The combined effect is a tongue of negative AOU anomalies in the ETP extending along the coast on either side of the equator (Figures 8b–8f). As the decay phase settles in around the peak of the ENSO event (Figure 6b), a strong reduction in the intensity of the trade winds across the Pacific causes the ECC to weaken, thus reducing the supply of low AOU waters and breaking up the AOU anomaly into two hemispheric blocks (Figures 8g–8e). The AOU anomalies are further transported westward on either side of the equator by the anomalous ocean circulation.

In addition, an intensification of the circulation in and out of the North Pacific ODZ on its poleward side leads to an increase in the curvature of the ODZ boundary, resulting in a dipole pattern change in AOU (Figures 8b–8f). This dipole change in AOU explains the spatially heterogeneous response of the oxycline in the ETNP (Figure 4c). This additional advective pathway continues to strengthen following the Niño 3.4 index peak explaining in parts the higher correlation of ODZ volume anomalies in the ETNP with a 3 month lag.

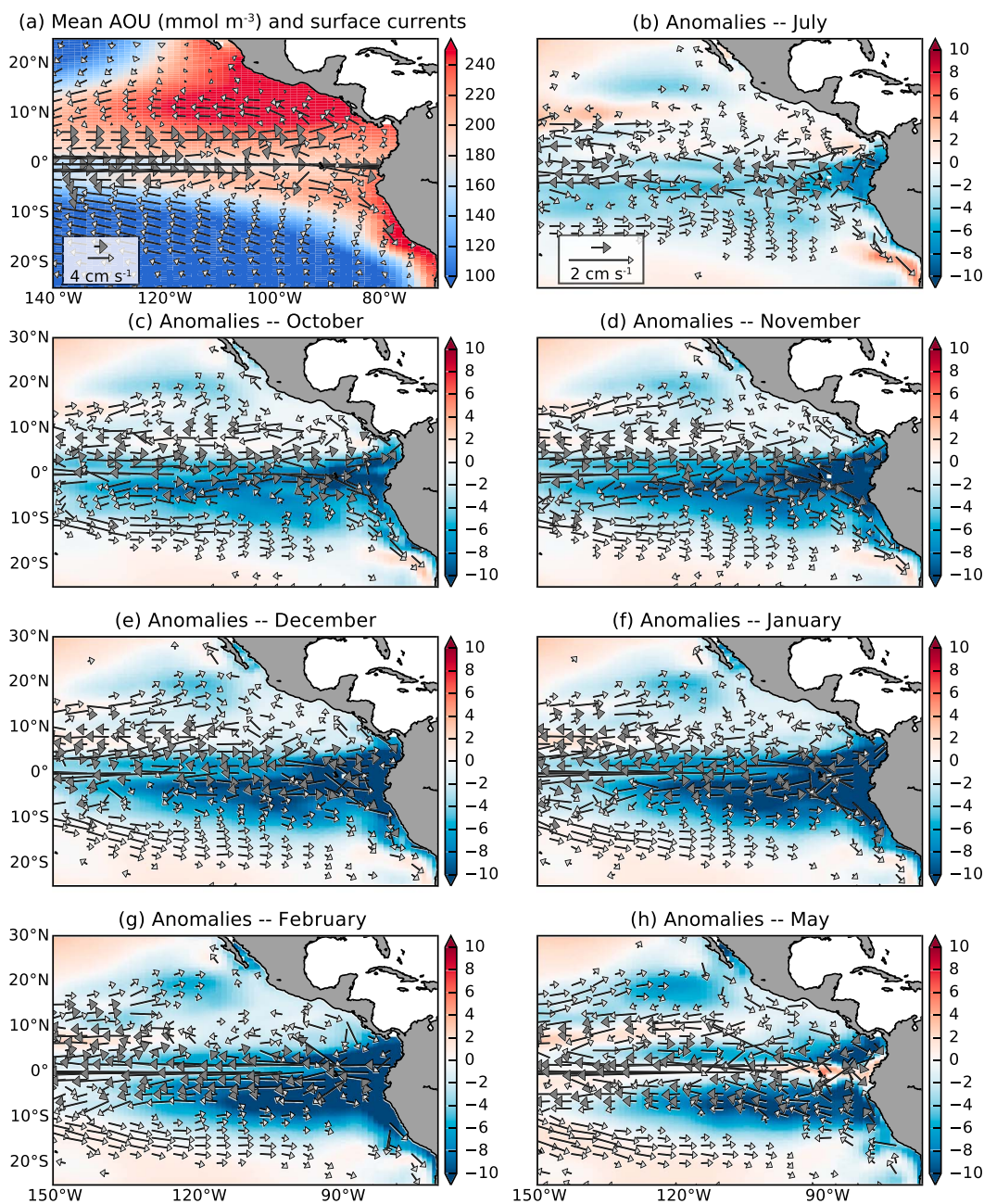


Figure 8. ENSO-composited monthly evolution of AOU and ocean current speed anomalies on the isopycnal $\sigma_0=26.8$. (a) Mean AOU (mmol m^{-3}) as colors and mean ocean current speed (cm s^{-1}) as vectors. (b–h) ENSO-composited monthly AOU anomalies (mmol m^{-3}) as colors and current speed anomalies (cm s^{-1}) as arrows for the indicated month.

Overall, the complex equatorial circulation response in the upper water column to ENSO-driven changes in wind stress causes large decreases in AOU (increases in O_2), resulting in the reduction of the extent of the ODZs and the deepening of their oxycline.

In summary, ENSO-associated changes in tropical wind trigger a series of positively reinforcing effects that together result in a strong response of WCD to ENSO in both the ETSP and ETNP. The winds play a central role in driving changes in ocean circulation and mixing, which affects both the oxygenation of the upper ocean as well as the changes in primary and export production, which then determine the demand for oxidants in this system. The strong amplification of the initial signal is largely the response to the near exponential decay with depth of the rate of remineralization, such that an upper ocean change in the oxic/suboxic boundary

leads to large changes in water column denitrification. Such a large response in WCD, i.e., over 70% of its mean rate between a peak El Niño and a peak La Niña event, is bound to have implications for the Pacific N cycle. Before investigating those, we discuss our results in the light of past studies, as well as their robustness.

4.4. Robustness of the Findings

To our knowledge, so far only Deutsch et al. (2011) have discussed interannual variability of WCD in the Eastern Tropical Pacific. These authors limited their analyses to the ETNP but found an ENSO-driven variability of WCD that is remarkably similar in magnitude and timing as simulated in our study. For example, they simulate an increase of over 70% of the mean North Pacific WCD between the 1998 El Niño and the 1999 La Niña episodes, consistent with our findings (Figure 3a). However, even though it is encouraging to note that both models exhibit similar WCD variability, the following sources of uncertainties need to be taken into account when evaluating our results: (i) uncertainties associated with our parameterization of N losses, (ii) errors associated with the potential misrepresentation of the variability of organic carbon remineralization, and (iii) errors associated with the representation of the variability of ODZ geometry.

A first potential source of error is the absence of anammox as a N loss pathway in our biogeochemical model. Babbin et al. (2014) showed that the total N loss is tightly controlled by the flux of organic matter through the ODZ. WCD in our simulation can therefore be seen as an N loss term that encompasses both anammox and denitrification. A second source of error is the potential misrepresentation of the variability of the remineralization field due to biases in the simulation of NPP or in the representation of the organic matter transfer efficiency. Our model simulates an increase in NPP over the climatological extent of the ODZ in the ETNP of close to 20% from 1998 to 2000, smaller than the 35% increase in NPP reconstructed from satellite chl-a (Figure S3d). Over the same time period, simulated organic matter export at 100 m over the ODZ in the ETNP increased by 40% in our simulation, which is significantly smaller than the 120% increase seen in the satellite-based estimate of Dunne et al. (2007; Figure S4d). In contrast, the simulated increase in NPP and export over the extent of the ODZ in the ETSP compares well with satellite-based reconstructions (Figures S3e and S4e). Therefore, given the important role of remineralization rates in driving the response of WCD in the ETNP (Figure 5), our model may underestimate the ENSO-driven response there. Overall, however, the simulation of ENSO-related NPP changes appears reasonable based on the limited information available. Finally, a misrepresentation of the complex equatorial circulation can lead to biases in the ventilation of the ODZs. Coarse ocean models usually do not resolve subsurface countercurrents that mark the separation between the better ventilated tropics and the ODZs well (Cabre et al., 2015). In our model, this was partially accounted for by increasing isopycnal mixing along the equator, enabling us to simulate more realistic ODZ volumes in the mean state. We acknowledge that such an ad hoc parameterization only improves the mean simulated distribution of O₂ and does only allow for a relatively static response of these secondary jets to ENSO. However, as shown in sections 4.1 and 4.2, WCD is most sensitive to change in O₂ in the upper part of the water column where rates of remineralizations are high, and where the equatorial circulation is most dynamic. Based on our analysis of these potential caveats, we conclude that in our simulation, the mechanism by which WCD is modulated by ENSO, and the large magnitude of its response are robust results.

4.5. Implications of a High Interannual Variability in WCD

The large fluctuations of Pacific WCD simulated in this study have important implications for the marine N cycle, both regionally and globally (Gruber, 2008). This is particularly relevant since many aspects of the N cycle are only relatively poorly observed and quantified, yet model simulations suggested that major changes may lay ahead. We consider here three topics, (i) the implication for the interpretation of regional rates and changes in the ETP, (ii) the implication for the global marine N budget, and (iii) the implications for the global marine production of the greenhouse gas N₂O.

There is a broad consensus that tropical O₂ in the Pacific will decline in response to climate change (Bopp et al., 2013; Cocco et al., 2013; Keeling et al., 2010), potentially leading to an increase in ODZ volume and WCD. In addition, it has been shown that the ODZ volume may have expanded over the past three decades, probably in response to decadal climate variations, but possibly also as a harbinger of future climate change (Deutsch et al., 2011, 2014; Ito & Deutsch, 2013). This has led the community to intensify efforts to assess trends in O₂ concentrations as well as other tracers impacted by a decrease in O₂ such as nitrite and N*, modified through changes in denitrification. For example, Horak et al. (2016) used four snapshot sections of N* and nitrite in the ETNP to show that over the past 30 years, the extent of anoxia expanded vertically and that WCD increased. Our results suggest that trends calculated from a very limited number of temporal

snapshots may be prone to large errors, especially when based on measurements, taken during strong El Niño or La Niña episodes.

Highly variable WCD on interannual timescales is bound to impact the balance of the global marine N budget. While, there is strong evidence that feedbacks in the N cycle prevent large variations in the marine N inventory on centennial and longer timescales (Canfield et al., 2010; Gruber, 2004; Deutsch, 2004), this may not be the case on shorter timescales. This is because those feedbacks are thought to operate through a response of inputs (N fixation) or outputs (denitrification) to deficiencies or excesses in oceanic N^* caused by a perturbation of the N cycle (Gruber, 2004, 2008). On interannual timescales, denitrification-induced N^* anomalies cannot be transported fast enough to the surface to generate a global response of N fixation. Our large simulated variability of WCD therefore suggests that the Pacific marine N budget constantly exhibits large imbalances. In fact, we simulate a temporary imbalance of the Pacific marine N budget of over 20% of total nitrogen turnover during a strong El Niño or La Niña year.

Finally, our result also suggest the presence of rather strong year-to-year fluctuations in the marine emissions of N_2O . This is because more than half of all marine N_2O emissions may be produced during an intermediate step of denitrification (Babbin et al., 2014). Differing O_2 thresholds for the production and consumption of N_2O (Betlach & Tiedje, 1981; Korner & Zumft, 1989) may cause a large residual N_2O production along the oxycline in the ODZs (Babbin et al., 2015). Thus, the implications of our result are twofold. First, a large interannual variability of WCD implies that net N_2O production may also exhibit large interannual variations. Furthermore, N_2O produced through this pathway is a residual of significantly larger production and consumption rates, making its net production highly sensitive to changes in ODZ geometry. Thus, N_2O has the potential for an even stronger response than denitrification, with large production pulses during La Niñas and minimum production during El Niño episodes.

5. Conclusion

We simulated a strong response of WCD in the Pacific Ocean to ENSO variability. More specifically, ENSO-associated changes in wind patterns drive a series of responses that act together to modify export production and ODZ geometry in such a way that the response of WCD is strongly amplified. The large interannual variability of WCD has multiple implications. First, estimating trends in the rates of WCD (or other related quantities) from snapshot measurements will be difficult, given their potential multiyear variation of over 70%. Second, because stabilizing feedbacks of the marine N cycle operate on timescales much larger than the simulated variability, the marine N budget probably exhibits very large imbalances on interannual timescales. Finally, N_2O emissions, because of their tight relation to denitrification rates and ODZ geometry, probably also exhibit large interannual variations.

Acknowledgments

This research was funded by ETH Zürich. Keith Moore is thanked for sharing his modifications to the NCAR CESM code and for helpful discussions. We also thank Tim Devries and an anonymous reviewer for their constructive comments that helped to improve the manuscript. Model output is available upon request to the corresponding author (simon.yang.ch@gmail.com). All other data used in this study are listed in the references.

References

- Babbin, A. R., Bianchi, D., Jayakumar, A., & Ward, B. B. (2015). Rapid nitrous oxide cycling in the suboxic ocean. *Science*, *348*(6239), 1127–1129.
- Babbin, A. R., Keil, R. G., Devol, A. H., & Ward, B. B. (2014). Organic matter stoichiometry, flux, and oxygen control nitrogen loss in the ocean. *Science*, *344*(6182), 406–408. <https://doi.org/10.1126/science.1248364>
- Balmaseda, M. A., Mogensen, K., & Weaver, A. T. (2013). Evaluation of the ECMWF ocean reanalysis system ORAS4. *Quarterly Journal of the Royal Meteorological Society*, *139*(674), 1132–1161. <https://doi.org/10.1002/qj.2063>
- Belmadani, A., Echevin, V., Dewitte, B., & Colas, F. (2012). Equatorially forced intraseasonal propagations along the Peru-Chile coast and their relation with the nearshore eddy activity in 1992–2000: A modeling study. *Journal of Geophysical Research*, *117*, C04025. <https://doi.org/10.1029/2011JC007848>
- Betlach, M. R., & Tiedje, J. M. (1981). Kinetic explanation for accumulation of nitrite, nitric oxide, and nitrous oxide during bacterial denitrification. *Applied and Environmental Microbiology*, *42*(6), 1074–1084.
- Bianchi, D., Dunne, J. P., Sarmiento, J. L., & Galbraith, E. D. (2012). Data-based estimates of suboxia, denitrification, and N_2O production in the ocean and their sensitivities to dissolved O_2 . *Global Biogeochemical Cycles*, *26*, GB2009. <https://doi.org/10.1029/2011GB004209>
- Bopp, L., Resplandy, L., Orr, J. C., Doney, S. C., Dunne, J. P., Gehlen, M., ... Vichi, M. (2013). Multiple stressors of ocean ecosystems in the 21st century: Projections with CMIP5 models. *Biogeosciences*, *10*(10), 6225–6245. <https://doi.org/10.5194/bg-10-6225-2013>
- Cabre, A., Marinov, I., Bernardello, R., & Bianchi, D. (2015). Oxygen minimum zones in the tropical Pacific across CMIP5 models: Mean state differences and climate change trends. *Biogeosciences*, *12*(18), 5429–5454. <https://doi.org/10.5194/bg-12-5429-2015>
- Canfield, D. E., Glazer, A. N., & Falkowski, P. G. (2010). The evolution and future of Earth's nitrogen cycle. *Science*, *330*(6001), 192–196. <https://doi.org/10.1126/science.1186120>
- Capotondi, A., Wittenberg, A. T., Newman, M., Di Lorenzo, E., Yu, J.-Y., Braconnot, P., ... Guilyardi, E. (2015). Understanding ENSO diversity. *Bulletin of the American Meteorological Society*, *96*(6), 921–938.
- Castro, C. G., Chavez, F. P., & Collins, C. A. (2001). Role of the California Undercurrent in the export of denitrified waters from the Eastern Tropical North Pacific. *Global Biogeochemical Cycles*, *15*(4), 819–830. <https://doi.org/10.1029/2000GB001324>

- Chaigneau, A., Dominguez, N., Eldin, G., Vasquez, L., Flores, R., Grados, C., & Echevin, V. (2013). Near-coastal circulation in the Northern Humboldt Current System from shipboard ADCP data. *Journal of Geophysical Research: Oceans*, *118*, 5251–5266. <https://doi.org/10.1002/jgrc.20328>
- Chavez, F. P., Collins, C. A., Huyer, A., & Mackas, D. L. (2002). El Niño along the West Coast of North America. *Progress in Oceanography*, *54*(1–4), 1–5. [https://doi.org/10.1016/S0079-6611\(02\)00040-X](https://doi.org/10.1016/S0079-6611(02)00040-X)
- Chavez, F. P., Pennington, J. T., Castro, C. G., Ryan, J. P., Michisaki, R. P., Schlining, B., ... Collins, C. A. (2002). Biological and chemical consequences of the 1997–1998 El Niño in central California waters. *Progress in Oceanography*, *54*(1), 205–232. [https://doi.org/10.1016/S0079-6611\(02\)00050-2](https://doi.org/10.1016/S0079-6611(02)00050-2)
- Chen, X., Qiu, B., Du, Y., Chen, S., & Qi, Y. (2016). Interannual and interdecadal variability of the North Equatorial Countercurrent in the western Pacific. *Journal of Geophysical Research: Oceans*, *121*, 7743–7758. <https://doi.org/10.1002/2016JC012190>
- Cocco, V., Joos, F., Steinacher, M., Frölicher, T. L., Bopp, L., Dunne, J., ... Tjiputra, J. (2013). Oxygen and indicators of stress for marine life in multi-model global warming projections. *Biogeosciences*, *10*(3), 1849–1868. <https://doi.org/10.5194/bg-10-1849-2013>
- Danabasoglu, G., Bates, S. C., Briegleb, B. P., Jayne, S. R., Jochum, M., Large, W. G., ... Yeager, S. G. (2011). The CCSM4 ocean component. *Journal of Climate*, *25*(5), 1361–1389. <https://doi.org/10.1175/JCLI-D-11-00091.1>
- Deser, C., Phillips, A. S., Tomas, R. A., Okumura, Y. M., Alexander, M. A., Capotondi, A., ... Ohba, M. (2012). ENSO and Pacific decadal variability in the Community Climate System Model version 4. *Journal of Climate*, *25*(8), 2622–2651. <https://doi.org/10.1175/JCLI-D-11-00301.1>
- Deutsch, C. (2004). Isotopic constraints on glacial/interglacial changes in the oceanic nitrogen budget. *Global Biogeochemical Cycles*, *18*, GB4012. <https://doi.org/10.1029/2003GB002189>
- Deutsch, C., Gruber, N., Key, R. M., Sarmiento, J. L., & Ganachaud, A. (2001). Denitrification and N₂ fixation in the Pacific Ocean. *Global Biogeochemical Cycles*, *15*(2), 483–506.
- Deutsch, C., Brix, H., Ito, T., Frenzel, H., & Thompson, L. (2011). Climate-forced variability of ocean hypoxia. *Science (New York, N.Y.)*, *333*(6040), 336–9. <https://doi.org/10.1126/science.1202422>
- Deutsch, C., Berelson, W., Thunell, R., Weber, T., Tems, C., McManus, J., ... van Geen, A. (2014). Centennial changes in North Pacific anoxia linked to tropical trade winds. *Science*, *345*(6197), 665–668. <https://doi.org/10.1126/science.1252332>
- DeVries, T., Deutsch, C., Primeau, F., Chang, B., & Devol, A. (2012). Global rates of water-column denitrification derived from nitrogen gas measurements. *Nature Geoscience*, *5*, 547–550. <https://doi.org/10.1038/ngeo1515>
- DeVries, T., Deutsch, C., Rafter, P. A., & Primeau, F. (2013). Marine denitrification rates determined from a global 3-D inverse model. *Biogeosciences*, *10*(4), 2481–2496. <https://doi.org/10.5194/bg-10-2481-2013>
- Di Lorenzo, E., Schneider, N., Cobb, K. M., Franks, P. J. S., Chhak, K., Miller, A. J., & Riviere, P. (2008). North Pacific Gyre Oscillation links ocean climate and ecosystem change. *Geophysical Research Letters*, *35*, L08607. <https://doi.org/10.1029/2007GL032838>
- Dunne, J. P., Sarmiento, J. L., & Gnanadesikan, A. (2007). A synthesis of global particle export from the surface ocean and cycling through the ocean interior and on the seafloor. *Global Biogeochemical Cycles*, *21*, GB4006. <https://doi.org/10.1029/2006GB002907>
- Frischknecht, M., Münnich, M., & Gruber, N. (2015). Remote versus local influence of ENSO on the California Current System. *Journal of Geophysical Research: Oceans*, *120*, 1353–1374. <https://doi.org/10.1002/2014JC010531>
- Frölicher, T. L., Joos, F., Plattner, G. K., Steinacher, M., & Doney, S. C. (2009). Natural variability and anthropogenic trends in oceanic oxygen in a coupled carbon cycle-climate model ensemble. *Global Biogeochemical Cycles*, *23*, GB1003. <https://doi.org/10.1029/2008GB003316>
- Fuenzalida, R., Schneider, W., Garcés-Vargas, J., Bravo, L., & Lange, C. (2009). Vertical and horizontal extension of the oxygen minimum zone in the eastern south Pacific Ocean. *Deep Sea Research Part II: Topical Studies in Oceanography*, *56*(16), 992–1003. <https://doi.org/10.1016/j.dsr2.2008.11.001>
- Gent, P. R., Danabasoglu, G., Donner, L. J., Holland, M. M., Hunke, E. C., Jayne, S. R., ... Zhang, M. (2011). The Community Climate System Model version 4. *Journal of Climate*, *24*, 4973–4991. <https://doi.org/10.1175/2011JCLI4083.1>
- Getzlaff, J., & Dietze, H. (2013). Effects of increased isopycnal diffusivity mimicking the unresolved equatorial intermediate current system in an Earth system climate model. *Geophysical Research Letters*, *40*, 2166–2170. <https://doi.org/10.1002/grl.50419>
- Graco, M., Purca, S., Dewitte, B., Morón, O., Ledesma, J., Flores, G., ... Gutiérrez, D. (2016). The OMZ and nutrients features as a signature of interannual and low frequency variability off the Peruvian upwelling system. *Biogeosciences Discussions*, 1–36. <https://doi.org/10.5194/bg-2015-567>
- Griffes, S., Winton, M., Samuels, B., & Danabasoglu, G. (2011). The CORE datasets from Large and Yeager for use in forcing global ocean-ice simulations, Go-Essp.Gfdl.Noaa.Gov (pp. 1–12).
- Gruber, N. (2004). The dynamics of the marine nitrogen cycle and its influence on atmospheric CO₂ variations. In M. Follows, & T. Oguz (Eds.), *The ocean carbon cycle and climate* (Vol. 40, pp. 97–148). Dordrecht: Kluwer Academic. https://doi.org/10.1007/978-1-4020-2087-2_4
- Gruber, N. (2008). The marine nitrogen cycle: Overview and challenges. In D. G. Capone, et al. (Eds.), *Nitrogen in the marine environment* (Chap. 1, pp. 1–50). Amsterdam: Elsevier.
- Gruber, N., & Sarmiento, J. L. (1997). Global patterns of marine nitrogen fixation and denitrification. *Global Biogeochemical Cycles*, *11*(2), 235–266. <https://doi.org/10.1029/97GB00077>
- Hamme, R. C., & Emerson, S. R. (2006). Constraining bubble dynamics and mixing with dissolved gases: Implications for productivity measurements by oxygen mass balance. *Journal of Marine Research*, *64*(1), 73–95.
- Hamme, R. C., & Severinghaus, J. P. (2007). Trace gas disequilibria during deep-water formation. *Deep Sea Research Part I: Oceanographic Research Papers*, *54*(6), 939–950. <https://doi.org/10.1016/j.dsr.2007.03.008>
- Hermann, A. J., Curchitser, E. N., Haidvogel, D. B., & Dobbins, E. L. (2009). A comparison of remote vs. local influence of El Niño on the coastal circulation of the northeast Pacific. *Deep Sea Research Part II: Topical Studies in Oceanography*, *56*(24), 2427–2443. <https://doi.org/10.1016/j.dsr2.2009.02.005>
- Horak, R. E. A., Ruef, W., Devol, A. H., & Ward, B. B. (2016). Expansion of denitrification and anoxia in the Eastern Tropical North Pacific from 1972 to 2012. *Geophysical Research Letters*, *43*, 5252–5260. <https://doi.org/10.1002/2016GL068871>
- Huang, B., Banzon, V. F., Freeman, E., Lawrimore, J., Liu, W., Peterson, T. C., ... Zhang, H.-M. (2014). Extended reconstructed sea surface temperature version 4 (ERSST.v4). Part I: Upgrades and intercomparisons. *Journal of Climate*, *28*(3), 911–930. <https://doi.org/10.1175/JCLI-D-14-00006.1>
- Ito, T., & Deutsch, C. (2013). Variability of the oxygen minimum zone in the tropical North Pacific during the late twentieth century. *Global Biogeochemical Cycles*, *27*, 1119–1128. <https://doi.org/10.1002/2013GB004567>
- Ito, T., Follows, M. J., & Boyle, E. A. (2004). Is AOU a good measure of respiration in the oceans? *Geophysical Research Letters*, *31*, L17305. <https://doi.org/10.1029/2004GL020900>
- Jochum, M., Danabasoglu, G., Holland, M., Kwon, Y.-O., & Large, W. G. (2008). Ocean viscosity and climate. *Journal of Geophysical Research*, *113*, C06017. <https://doi.org/10.1029/2007JC004515>

- Keeling, R. F., Körtzinger, A., & Gruber, N. (2010). Ocean deoxygenation in a warming world. *Annual Review of Marine Science*, 2(1), 199–229. <https://doi.org/10.1146/annurev.marine.010908.163855>
- Korner, H., & Zumft, W. G. (1989). Expression of denitrification enzymes in response to the dissolved oxygen level and respiratory substrate in continuous culture of *Pseudomonas stutzeri*. *Applied and Environmental Microbiology*, 55(7), 1670–1676.
- Large, W. G., & Yeager, S. G. (2009). The global climatology of an interannually varying air-sea flux data set. *Climate Dynamics*, 33(2–3), 341–364. <https://doi.org/10.1007/s00382-008-0441-3>
- Long, M. C., Deutsch, C., & Ito, T. (2016). Finding forced trends in oceanic oxygen. *Global Biogeochemical Cycles*, 30, 381–396. <https://doi.org/10.1002/2015GB005310>
- Montes, I., Colas, F., Capet, X., & Schneider, W. (2010). On the pathways of the equatorial subsurface currents in the eastern equatorial Pacific and their contributions to the Peru-Chile Undercurrent. *Journal of Geophysical Research*, 115, C09003. <https://doi.org/10.1029/2009JC005710>
- Moore, J. K., Doney, S. C., & Lindsay, K. (2004). Upper ocean ecosystem dynamics and iron cycling in a global three-dimensional model. *Global Biogeochemical Cycles*, 18, GB4028. <https://doi.org/10.1029/2004GB002220>
- Moore, J. K., Lindsay, K., Doney, S. C., Long, M. C., & Misumi, K. (2013). Marine ecosystem dynamics and biogeochemical cycling in the Community Earth System (Model CESM1(BGC)): Comparison of the 1990s with the 2090s under the RCP4.5 and RCP8.5 scenarios. *Journal of Climate*, 26(23), 9291–9312. <https://doi.org/10.1175/JCLI-D-12-00566.1>
- Paulmier, A., Kriest, I., & Oschlies, A. (2009). Stoichiometries of remineralisation and denitrification in global biogeochemical ocean models. *Biogeosciences*, 6(5), 923–935. <https://doi.org/10.5194/bg-6-923-2009>
- Rodgers, K. B., Lin, J., & Frölicher, T. L. (2015). Emergence of multiple ocean ecosystem drivers in a large ensemble suite with an Earth system model. *Biogeosciences*, 12(11), 3301–3320. <https://doi.org/10.5194/bg-12-3301-2015>
- Sarmiento, J. L., & Gruber, N. (2006). *Ocean biogeochemical dynamics*. Princeton, NJ: Princeton University Press.
- Stramma, L., Johnson, G. C., Sprintall, J., & Mohrholz, V. (2008). Expanding oxygen-minimum zones in the tropical oceans. *Science*, 320(5876), 655–658. <https://doi.org/10.1126/science.1153847>
- Stramma, L., Johnson, G. C., Firing, E., & Schmidtko, S. (2010). Eastern Pacific oxygen minimum zones: Supply paths and multidecadal changes. *Journal of Geophysical Research*, 115, C09011. <https://doi.org/10.1029/2009JC005976>
- Stramma, L., Fischer, T., Grundle, D. S., Krahnemann, G., Bange, H. W., & Marandino, C. A. (2016). Observed El Niño conditions in the eastern tropical Pacific in October 2015. *Ocean Science*, 12, 861–873. <https://doi.org/10.5194/os-12-861-2016>
- Yang, S., & Gruber, N. (2016). The anthropogenic perturbation of the marine nitrogen cycle by atmospheric deposition: Nitrogen cycle feedbacks and the ¹⁵N Haber-Bosch effect. *Global Biogeochemical Cycles*, 30, 1418–1440. <https://doi.org/10.1002/2016GB005421>